iScience

CellPress
OPEN ACCESS

Article

Hyperactivation of Hedgehog signaling impedes myelin development and repair via cholesterol dysregulation in oligodendrocytes

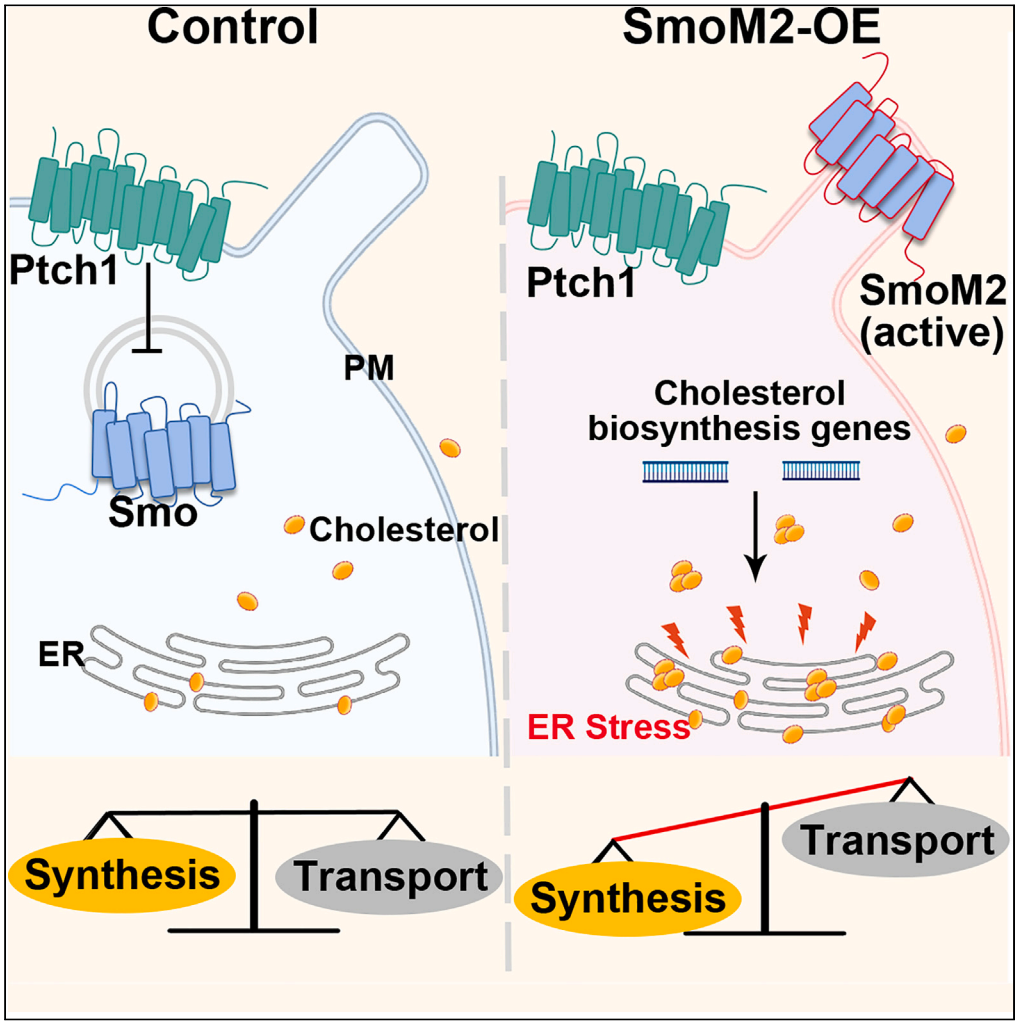

Minxi Fang, Xuan Wang, Lixia Chen, ..., Junlin Yang, Mengsheng Qiu, Xiaofeng Xu

msqiu@hznu.edu.cn (M.Q.)
xiaofengxu@hznu.edu.cn (X.X.)

Highlights

Hyperactivation of Hh signaling in OPCs suppresses myelination and remyelination

Hh signaling hyperactivation boosts cholesterol biosynthesis, disrupting homeostasis

Enhancing cholesterol transport reverses OL differentiation and myelination defects

Fang et al., iScience 27, 111016
October 18, 2024
https://doi.org/10.1016/j.isci.2024.111016

iScience

CellPress
OPEN ACCESS

Article

Hyperactivation of Hedgehog signaling impedes myelin development and repair via cholesterol dysregulation in oligodendrocytes

Minxi Fang,[1,2] Xuan Wang,[1,2] Lixia Chen,[2] Fang Li,[2] Sitong Wang,[2] Leyi Shen,[2] Huanyi Yang,[2] Lifen Sun,[2] Xue Wang,[2] Junlin Yang,[2] Mengsheng Qiu,[1,2,*] and Xiaofeng Xu[2,3,*]

SUMMARY

The failure to remyelinate demyelinated axons poses a significant challenge in the treatment of multiple sclerosis (MS), a chronic inflammatory demyelinating disease of the central nervous system. Here, we investigated the role of Hedgehog (Hh) signaling in myelin formation during development and under pathological conditions. Using conditional gain-of-function analyses, we found that hyperactivation of Hh signaling in oligodendrocyte precursor cells (OPCs) inhibits oligodendrocyte (OL) differentiation and myelination. Notably, sustained activation of Hh signaling in adult OPCs hinders myelin repair following LPC-induced focal demyelination. Through RNA sequencing, we discovered that genes associated with cholesterol synthesis were upregulated, and observed intracellular cholesterol accumulation in Hh-activated OPCs. Importantly, pharmacological stimulation of cholesterol transport was able to rescue the OL differentiation and myelination defects in mice. These findings establish a functional connection between Hh signaling, cholesterol homeostasis, and remyelination, providing insights for the strategic design of employing Hh signaling modulators in treating demyelinating neurodegenerative diseases.

INTRODUCTION

Oligodendrocytes (OLs) in the central nervous system (CNS) produce myelin sheaths around neuronal axons to promote the rapid transmission of action potentials,[1–3] provide metabolic supports and coordinate neural rhythms and activities.[4–6] During myelination, OL lineage goes through multiple developmental stages, including oligodendrocyte precursor cells (OPCs), newly formed OLs (NFOs) and mature OLs (MOLs).[7–11] Defective myelination has been implicated in cognitive deficits and motor learning. Failure of OLs to remyelinate demyelinated axons leads to irreversible axonal degeneration in demyelinated diseases (e.g., multiple sclerosis, MS).[12–15] OL differentiation and myelination are regulated by an intrinsic interplay of epigenetic regulators, transcriptional factors, and extracellular signals.[16] Understanding the signaling pathways governing oligodendrocyte differentiation and myelination is essential for devising therapeutic approaches aimed at repairing myelin in demyelinated disorders.

Earlier extensive research has consistently suggested that the Hedgehog (Hh) signaling pathway plays a vital role in the development of OLs.[17–19] During the early developmental phases, OPCs emerge from specific regions of the neuroepithelium within the ventricular zone (VZ). Subsequently, these cells migrate into adjacent areas, where they undergo proliferation and differentiation into mature, myelinating OLs. Genetic and molecular evidences support the notion that Hh signaling promotes OPC specification.[20] Smoothened (Smo) acts as a crucial mediator for transmitting Hh signaling across the plasma membrane.[21] In *Smo*$^{-/-}$ or *Shh*$^{-/-}$ mutants, the production of OPCs from neuroepithelial cells is inhibited.[22,23] Transplantation experiments have provided further evidence that Shh signaling induces the maturation of OPCs obtained from neurospheres originating from embryonic rat brain.[24,25] Additionally, Smo-mediated Hh signaling has been shown to significantly enhance the proliferation of neural progenitor cells (NPCs) and OPCs.[26–29] This effect is evident in experiments where adenovirus-mediated delivery of Shh into the lateral ventricle of adult mice results in increased cell proliferation.[26] Recently, Laouarem et al. demonstrated that pharmacological activation of Smo increases OPC proliferation and inhibits their differentiation, whereas inhibition of Smo enhances OPC differentiation, both *in vivo* and *in vitro*.[30] Furthermore, through activating Smo at distinct stages, we previously uncovered a stage-specific regulations of OL development by Hh signaling in the embryonic spinal cords.[31] While activation of Smo in NPCs could induce transient ectopic generation of OPCs and premature differentiation of OLs, sustained activation of Smo in committed OPCs primarily induces cell proliferation and concurrently suppresses their differentiation into OLs. However, the molecular mechanisms underlying the impaired OL

[1]College of Life Sciences, Zhejiang University, Hangzhou 310058, China
[2]Zhejiang Key Laboratory of Organ Development and Regeneration, College of Life and Environmental Sciences, Hangzhou Normal University, Hangzhou 311121, China
[3]Lead contact
*Correspondence: msqiu@hznu.edu.cn (M.Q.), xiaofengxu@hznu.edu.cn (X.X.)
https://doi.org/10.1016/j.isci.2024.111016

differentiation by Hh signaling activation remain to be elucidated, and the involvement of Hh signaling in myelin formation also awaits further investigation.

At the current stage, the role of the Hh pathway in remyelination remains somewhat controversial.[32] Wang et al. investigated the function of Shh-Gli1 pathway in human MS lesions, as well as in its animal model, experimental autoimmune encephalomyelitis (EAE).[33] They demonstrated that Shh is upregulated in MS and EAE lesions and induces neural stem cell (NSC) differentiation. Consequently, activators of the Hh signaling pathway, including Smo agonist such as SAG, have emerged as targets in treatment of MS,[34] as they can induce OPC proliferation and differentiation in the lesion sites of Cuprizone-induced demyelinating models.[35,36] However, it was previously reported that downregulation of Hh signaling is necessary for myelination during development, and enhanced Hh signaling causes a thinner corpus callosum in Gorlin syndrome patients.[37] In addition, Gli1, initially regarded as a reliable indicator of Hh pathway activity, has been found to have adverse effects during myelination/remyelination. Blocking Gli1 expression in the Cuprizone model was observed to enhance NPC recruitment, facilitate OPC migration toward demyelinated axons, and promote remyelination.[38,39] More recently, Nocera et al. utilized *Smo* loss-of-function and gain-of-function animal models and found that genetic activation of Smo increases the number of OPCs and decreases OL differentiation after Cuprizone treatment. Thus, their findings reveal that Hh signaling might function as a mitogen to encourage OPC proliferation, but does not facilitate myelination.[40] Given these contradictory findings, it is imperative to re-examine the function of Hh signaling activation in myelin repair and elucidate its underlying mechanism, as this line of study could guide the strategic design of utilizing Hh modulators for demyelinating disease treatments.

Our present work explores the role of the Hh signaling pathway in postnatal OL differentiation and (re)myelination processes. The research reveals that hyperactivation of Hh signaling specifically in OPCs hinders OL differentiation and myelination during developmental stages, which also obstructing myelin repair following demyelinating insults. The underlying mechanism involves the disruption of cholesterol synthesis and homeostasis caused by elevated Hh signaling in OPCs. Cholesterol is a vital component abundant in the myelin sheath. Notably, pharmacological enhancement of cholesterol transport has the potential to rectify the impairments in OL differentiation and myelination. In conclusion, our research establishes a functional link between Hh signaling, cholesterol homeostasis, and myelin repair, paving the way for strategic approaches in utilizing Hh signaling modulators for the treatment of demyelinating diseases.

RESULTS

Hyperactivation of Hh signaling in OPCs inhibits OL differentiation and myelination in the postnatal forebrain

To explore the role of Hh signaling in OL development, we generated double transgenic *PDGFRα^{creER}; SmoM2* (termed SmoM2-OE) mice by crossing *Rosa-SmoM2* with *PDGFRα-creER* mice. As previously documented, SmoM2, a missense mutation (W535L) of Smo, exhibits constitutive activation independent of the Hh ligand.[41] Tamoxifen was administrated intraperitoneally during the peak proliferation phase of brain OPCs, specifically from postnatal Day 5 to Day 7 (P5-P7), and analyzed at P15 (Figure 1A). To validate the specificity and efficacy of SmoM2 overexpression, we also performed a lineage tracing study by mating SmoM2-OE with the *Rosa-tdTomato* reporter line. Our findings revealed that all tdTomato-positive cells co-expressed SOX10 in both the cortex and corpus callosum (CC), indicating successful SmoM2 overexpression in OPCs (Figure 1B). Gene expression analyses via RNA *in situ* hybridization (ISH) showed significant downregulation of the myelin genes, *Mbp* and *Plp1*, in the CC and cortex of SmoM2-OE mice (Figures 1C and 1E). Immunostaining analyses further demonstrated a decrease in the number of CC1+ and ASPA+ mature OLs (Figures 1D and 1E). Therefore, constitutive activation of Hh signaling in OPCs impairs OL differentiation.

Additionally, we observed a notable increase in the number of *PDGFRα*+ OPCs in the cortex of SmoM2-OE mice compared to controls (Figures S1A and S1B). However, there was no significant difference in the distribution and number of total oligodendroglial cells labeled by SOX10 between SmoM2-OE and control mice (Figures S1C and S1D). Double immunostaining with SOX10 and the proliferation marker Ki67 indicated similar rates of OPC proliferation between SmoM2-OE and control mice (Figures S1E and S1F). To ensure that we did not miss the OPC proliferation period during the tamoxifen treatments, we conducted additional experiments with earlier tamoxifen administration at P2-4 followed by analysis at P12 (Figure S1G). Two hours before tissue collection, BrdU was injected to label proliferating cells. The results revealed no significant increase in the proportion of BrdU+ and Ki67+ cells in Sox10+ population between the control and mutant mice, aligning with our findings at P15 (Figures S1H and S1I). Based on these comprehensive results, we conclude that hyperactivation of Hh signaling in OPCs inhibits OL differentiation while having little or no effect on OPC proliferation and migration.

In light of the observed OL differentiation defects in SmoM2-OE mice, we conducted TrueGold staining to visualize the myelin fibers in the forebrain at P15. In control mice, we observed multiple dense and parallel axonal tracks, whereas the transgenic mice exhibited a notable decrease in TrueGold staining in these regions. Additionally, axonal fasciculation was largely absent, indicating compromised axonal myelination (Figures 2A and 2B). To further investigate the ultrastructure of myelin sheaths in the CC at P15, we employed transmission electron microscopy. As anticipated, the majority of axons in SmoM2-OE mice were found to be unmyelinated (Figures 2C and 2D), suggesting severe myelination impairement in these transgenic mice.

Hyperactivation of Hh signaling hinders remyelination

To further explore the impact of Hh signaling activation on remyelination, we induced focal demyelination by stereotactically injecting lysolecithin (LPC) into the CC of adult mice. This well-defined model allows us to study various phases of remyelination. In 8-week-old transgenic and control mice, tamoxifen was administrated for 5 days prior to injury, as well as 2 days post lesion (dpl) to trigger SmoM2 overexpression in both adult and newly formed OPCs (Figure 3A). To validate the efficiency of Cre recombination, we utilized the same tamoxifen injection

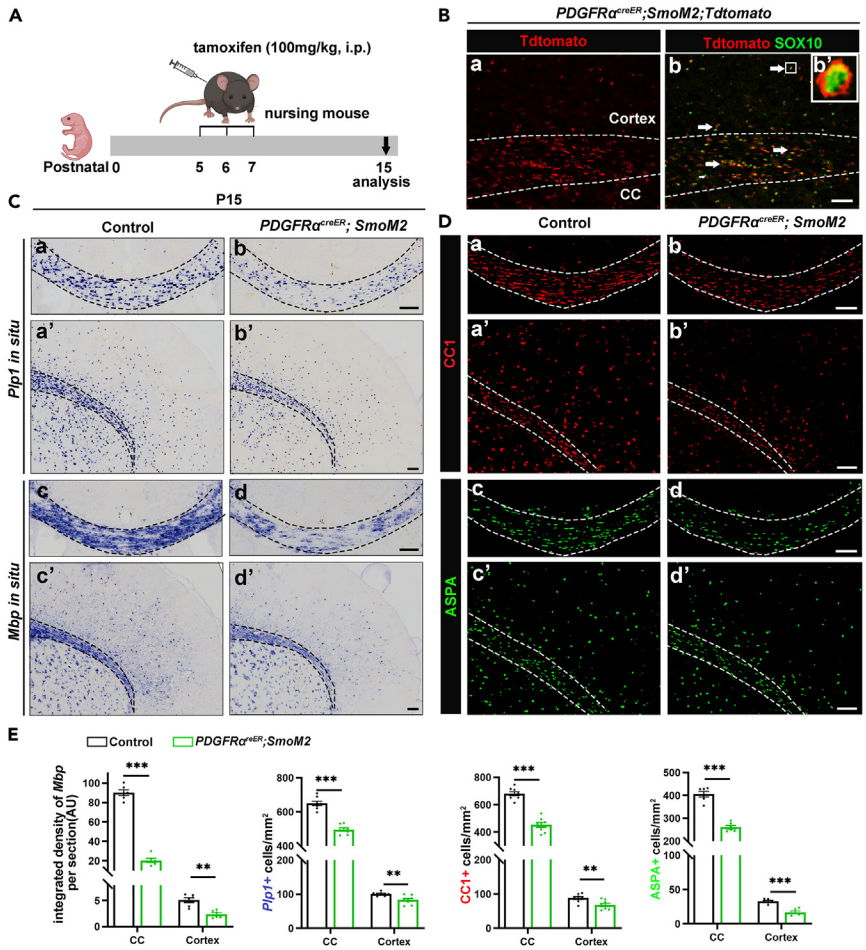

Figure 1. Hyperactivation of Hh signaling pathway inhibits OL differentiation after birth

(A) Experimental paradigm for tamoxifen injection in SmoM2-OE (*PDGFRα^{creER}; SmoM2*) and control mice.

(B) Immunostaining of tdTomato (red) and SOX10 (green) in the forebrain of *PDGFRα^{creER}; SmoM2; tdTomato* mice at P15. Arrows indicate colocalized tdTomato+/SOX10+ cell. b' shows the magnified view of the box in b.

(C) ISH of *Mbp* and *Plp1* in the CC and cortex of control and SmoM2-OE mice at P15. a, b, c and d show the middle of CC. a', b', c' and d' show the lateral CC and cortex.

(D) Immunostaining of CC1 (red) and ASPA (green) in the CC and cortex of control and SmoM2-OE mice at P15. a, b, c and d show the middle of CC. a', b', c' and d' show the lateral CC and cortex.

(E) Quantification of *Plp1+*, CC1+, ASPA+ OL density (calculated per mm2) and integrated density of *Mbp* (AU) from (C) and (D). Data are represented as mean ± *SEM*. For all statistical analysis, *p* values were calculated using unpaired t-tests. $^{**}p < 0.01$, $^{***}p < 0.001$. Scale bar: 100 μm.

paradigm in *Rosa-tdTomato; PDGFRα-CreER* mice. Our observations indicated that all tdtomato-positive cells co-expressed SOX10 in both the brain and the injury site, confirming the specific overexpression of SmoM2 in adult OPCs (Figures 3B and S2A).

The effects of induced Hh pathway activation on myelin maintenance in adult mice, was assessed by TrueGold myelin staining. In comparison to controls, no apparent differences were detected in myelin integrity within the uninjured cortex and corpus callosum of mutant mice (Figures S2B and S2C). Additionally, the initial LPC-induced injury was comparable between transgenic and control mice at 7dpl (Figures 3C and 3D). However, during the remyelination process, the lesion size on average decreased in control mice, whereas it remained significantly larger in SmoM2-OE mice at 14 and 21 dpl (Figures 3C and 3D). Thus, there was a substantial reduction in the density of newly formed myelin fibers in SmoM2-OE mice (Figures 3C and 3D), indicating that hyperactivation of SmoM2 impaired axonal remyelination.

Further examination of oligodendrocyte lineage markers at the lesion sites showed a similar density of *PDGFRα+* and SOX10+ cells between SmoM2-OE and control mice at 7 dpl (Figures 3E and 3F). Nevertheless, the density of newly formed OLs (*Plp1+* and ASPA+ cells) was significantly lower in SmoM2-OE mice compared to controls at 14 dpl and 21 dpl (Figures 3G, 3H, S2D, and S2E), suggesting a decreased capacity for OPC differentiation in SmoM2-OE mice relative to controls. Interestingly, most *PDGFRα+* and SOX10+ cells were non-proliferative (Ki67-) in both SmoM2-OE and control lesion sites, implying that Hh signaling activation did not augment OPC proliferation (Figures S2F

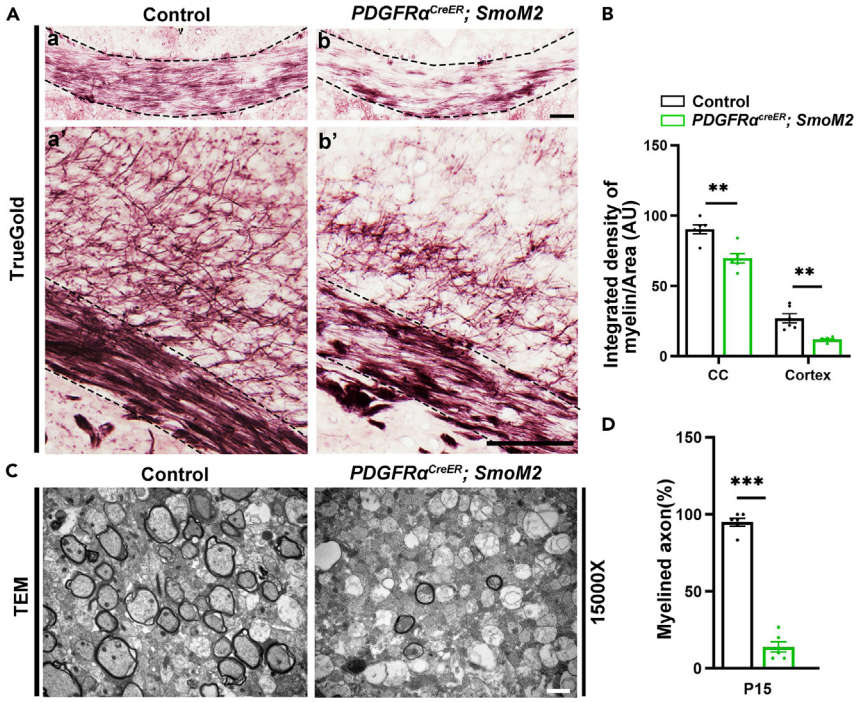

Figure 2. Hyperactivation of Hh signaling in OPCs impairs proper myelination

(A) TrueGold staining of myelin fibers in the CC and cortex of control and SmoM2-OE mice at P15. a and b show the middle CC. a' and b' show the lateral CC and cortex. Scale bar: 100 μm.

(B) Quantification of the density of myelin fibers per unit of area (μm^2) from (A).

(C) TEM analyses of myelin in the CC of control and SmoM2-OE mice at P15. Scale bar: 1 μm.

(D) Quantification of the percent of myelinated axons from (C). Data are represented as mean ± *SEM*. For all statistical analysis, *p* values were calculated using unpaired t-tests. $^{**}p < 0.01$, $^{***}p < 0.001$.

and S2G). These findings indicate that hyperactivation of Hh signaling in OPCs does not influence OPC recruitment to lesion sites following myelin injury, but significantly hinders oligodendrocyte differentiation and myelin repair.

Hyperactivation of Hh signaling leads to cholesterol accumulation in oligodendroglial cells

Given our findings that activation of Hh signaling in OPCs disrupts OL differentiation, myelination and remyelination, we aimed to pinpoint the downstream target genes and associated biological processes through bulk RNA sequencing (RNA-seq) in CC and cortex of P15 SmoM2-OE and control mice (Figure 4A). A total of 2,808 up-regulated and 2,474 down-regulated genes ($p < 0.05$) were identified in SmoM2-OE mice compared to their control littermates. In alignment with the differentiation defects observed in SmoM2-OE mice, we noted a significant downregulation of myelin genes, including *Mbp*, *Plp1*, *Mag*, *Cnp* and OL differentiation-associated genes, such as *Nkx2.2*, *Myrf*, *Id2* and *Ugt8a* (Figure 4C). Gene ontology (GO) analysis uncovered that the down-regulated genes are primarily involved in OL development and myelination, echoing the compromised OL differentiation in SmoM2-OE mice. Conversely, GO terms of up-regulated genes primarily concentrated on metabolic processes and stress responses (Figure 4B). Upon closer examination of metabolic processes, we found significant upregulation of genes encoding key enzymes involved in cholesterol biosynthesis, including *Scap*, *Srebf2*, *Mvd*, *Fdft1*, and *Mvk*, in SmoM2-OE mice (Figures 4C and 4D). The concurrent downregulation of myelin-related genes and upregulation of cholesterol homeostasis genes hinted at a possible link between hyperactivated Hh signaling and altered cholesterol homeostasis.

To visually assess cholesterol levels *in vivo*, we stained the cortex and CC with BODIPY-cholesterol. In SmoM2-OE mice, the BODIPY-staining appeared more intense than in control mice, with several larger cholesterol-accumulated lipid droplets observed, indicating of cholesterol accumulation (Figures S3A and S3B). To define the cell type with cholesterol accumulation, we co-stained BODIPY-cholesterol with distinct cell markers for OPCs (NG2), OLs (CC1), astrocytes (GFAP) and microglial (Iba1) in CC of both SmoM2-OE and control mice. Using confocal z stack microscopy for three-dimensional reconstruction, we observed no notable increase in BODIPY-cholesterol accumulation in Iba1+ microglia or GFAP+ astrocytes (Figures S3C, S3D, and 4G). By contrast, NG2+ and CC1+ oligodendroglial cells exhibited a significant increase in BODIPY-cholesterol punctuates (Figures 4E–4G), suggesting abnormal cholesterol accumulation in these cells with activated Hh signaling.

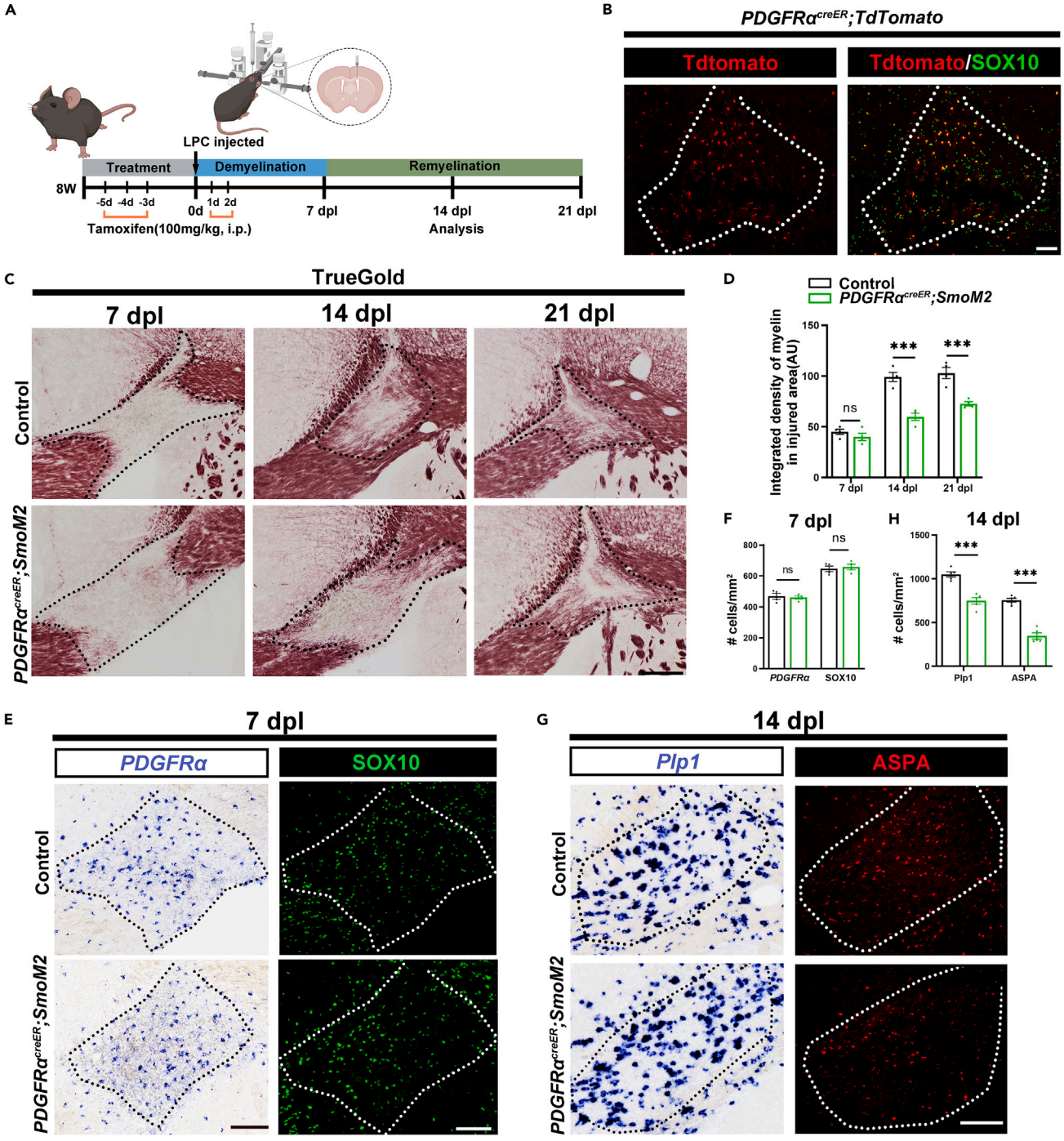

Figure 3. Hyperactivation of Hh signaling inhibits remyelination after LPC-induced focal demyelination

(A) Experimental paradigm of Tamoxifen and LPC injection in control and SmoM2-OE mice.

(B) Immunostaining of tdTomato (red) and SOX10 (green) in the injury lesion of *PDGFRα^{creER};tdTomato* mice at 9W.

(C) Representative image of TrueGold staining in the LPC injury sites from control and SmoM2-OE mice at 7, 14 and 21 dpl, respectively. Scale bar: 100μm.

(D) Quantification of the myelin density in the injury area (μm^2) at 7, 14 and 21 dpl from (C).

(E) ISH of *PDGFRα* and immunostaining of SOX10 in the injury sites of control and SmoM2-OE mice at 7 dpl.

(F) Quantification of *PDGFRα*+ and SOX10+ cell density per mm^2 in the injury sites of control and SmoM2-OE mice at 7 dpl from (E).

(G) ISH of *Plp1* and immunostaining of ASPA and SOX10 in the injury sites of control and SmoM2-OE mice at 14 dpl.

(H) Quantification of *Plp1*+ and ASPA+ cell density per mm^2 at 14 dpl from (G). Data are represented as mean ± *SEM*. For all statistical analysis, *p* values were calculated using unpaired t-tests. ***$p < 0.001$, ns: no significant difference. Scale bar: 100 μm.

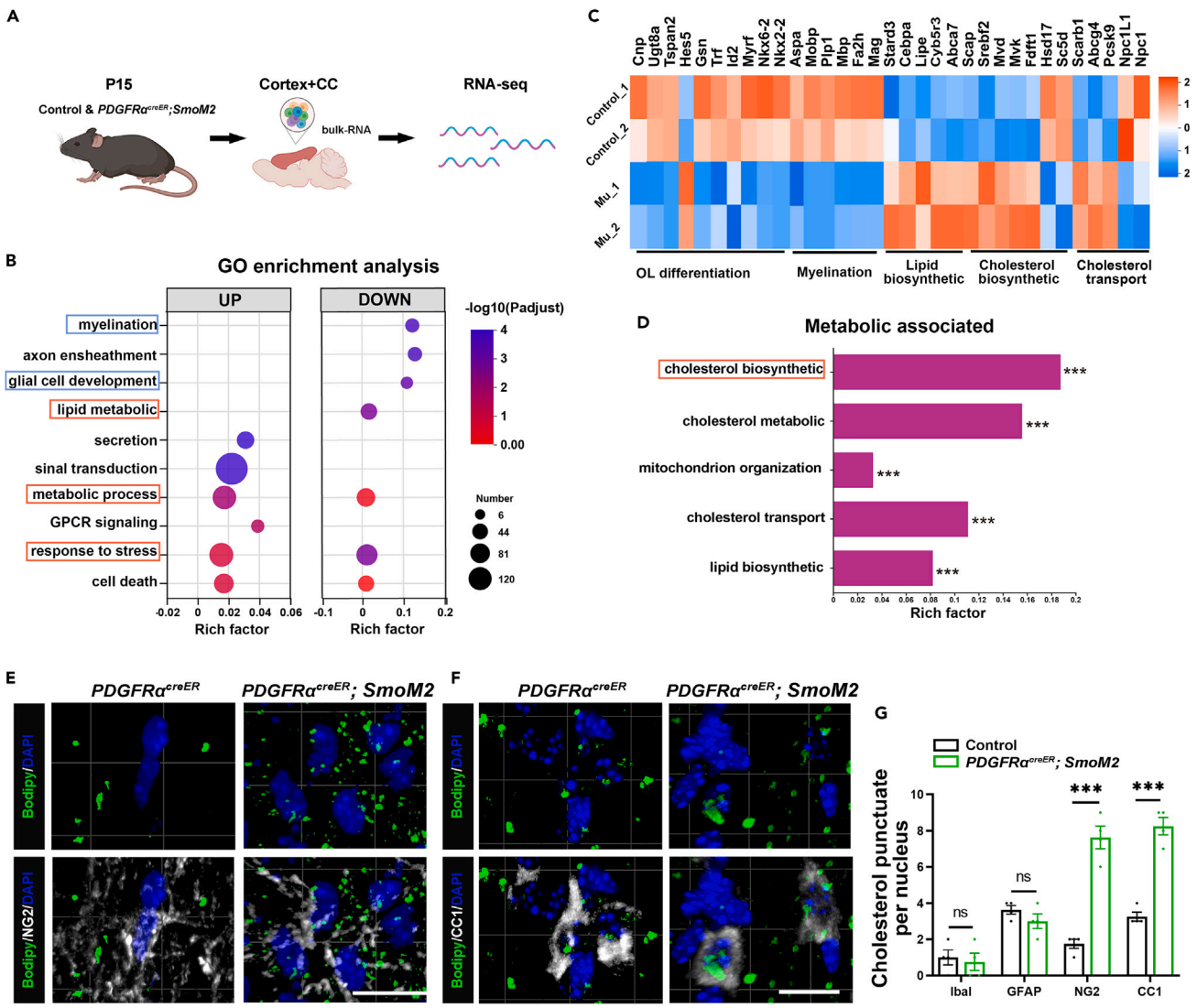

Figure 4. Hyperactivation of Hh signaling leds to cholesterol accumulation in oligodendroglial cells

(A) Experimental paradigm of bulk RNA-sequencing of CC and cortex tissues from control and SmoM2-OE mice.

(B) GO enrichment analysis of DEG. Biological processes of interest are highlighted in frame.

(C) DEG heatmap of distinct biological processes associated genes.

(D) Specific metabolic associated pathways with DEGs.

(E) Confocal 3D reconstruction of BODIPY-cholesterol staining alone or in combination with NG2 (white) in the CC from control and SmoM2-OE mice at P15.

(F) Confocal 3D reconstruction of BODIPY-cholesterol staining alone or in combination with CC1 (white) in the CC from control and SmoM2-OE mice at P15.

(G) Quantification of BODIPY-cholesterol punctuate in different cell types. Data points represent the mean of independent biological replicates. Data are represented as mean ± *SEM*. For all statistical analysis, *p* values were calculated using unpaired t-tests. ***$p < 0.001$. ns: no significant difference. Scale bar: 10 μm.

Pharmacologically enhancing cholesterol transport restores OL development and myelination

Given that hyperactivation of Hh signaling in OPCs leads to cholesterol accumulation, thereby hindering OL differentiation and myelination, we hypothesized that facilitating cholesterol transport might mitigate intracellular cholesterol accumulation. This, in turn, could potentially alleviate the differentiation defects observed in SmoM2-OE mice. To test this possibility, we employed 2-hydroxypropyl-β-cyclodextrin (HPβCD), a compound known bind cholesterol and facilitate its transport.[42–44] Following tamoxifen treatment, SmoM2-OE mice received intraperitoneal injections of either HPβCD or PBS for three consecutive days and were then analyzed at P15 (Figure 5A). In *SmoM2-OE; Rosa-tdTomato* mice treated with HPβCD, BODIPY-cholesterol droplets notably diminished in NG2+/tdTomato+ OPCs (indicating activated Hh signaling), suggesting a decline in cholesterol accumulation (Figures 5B and 5C). Immunostaining analyses revealed a significant increase in the density of CC1+ and ASPA+ cells in the CC and cortex of SmoM2-OE mice after HPβCD treatment (Figures 5D–5F). Similarly, TrueGold

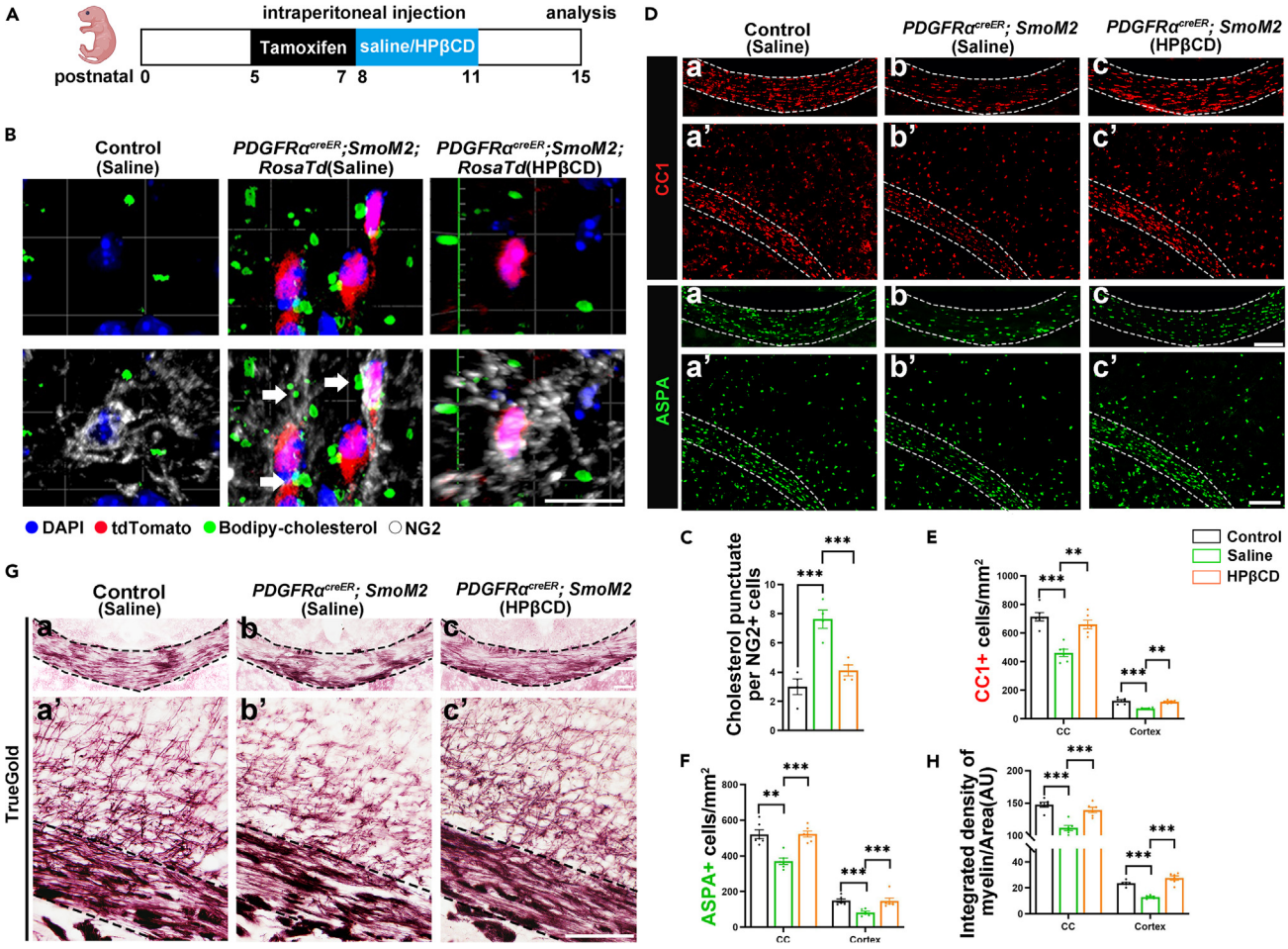

Figure 5. Facilitating cholesterol transport rescues OL differentiation and myelination defects in SmoM2-OE mice

(A) Experimental paradigm for tamoxifen and saline/HPβCD injection in control and SmoM2-OE mice.

(B) Confocal co-labeling of BODIPY-cholesterol, tdTomato and NG2 in the forebrain of control and SmoM2-OE mice with or without HPβCD injection at P15. Arrows highlight BODIPY-cholesterol accumulation around nuclei of tdTomato+/NG2+ cells. Scale bar: 10 μm.

(C) Quantification of cholesterol punctuate in NG2+ cells per nucleus from (B).

(D) Immunostaining of CC1 (red) and ASPA (green) in the CC and cortex of control and SmoM2-OE mice with or without HPβCD injection at P15. a, b and c show the middle of CC. a′, b′ and c′ show the lateral CC and cortex. Scale bar: 100 μm.

(E) Quantification of CC1+ OL density (calculated per mm^2) from (D).

(F) Quantification of ASPA+ mature OL density (calculated per mm^2) from (D).

(G) TrueGold staining of myelin fibers in the CC and cortex of control and SmoM2-OE mice with or without HPβCD injection at P15. a, b and c show the middle CC. a′, b′ and c′ show the lateral CC and cortex. Scale bar: 100 μm.

(H) Quantification of the density of myelin fibers per unit of area (μm2) from (G). Data are represented as mean ± *SEM*. For all statistical analysis, *p* values were calculated using one-way ANOVA with Dunnett's multiple-comparison correction. $^{**}p < 0.01$, $^{***}p < 0.001$.

myelin staining analyses confirmed an augmented density of myelin fibers and enhanced myelination in HPβCD-treated SmoM2-OE mice compared to untreated SmoM2-OE mice (Figures 5G and 5H). In conclusion, our findings demonstrated that hyperactivation of Hh signaling in OPCs disrupts OL differentiation and myelination primarily due to abnormal cholesterol accumulation in oligodendroglial cells. Importantly, pharmacological enhancement of cholesterol transport can significantly rescue these OL differentiation and myelination defects.

Cholesterol accumulation triggers ER stress in OPCs

To elucidate the mechanisms that underlie Hh-induced cholesterol accumulation and subsequent OL differentiation defects, we treated CG4 oligodendroglial cell line with SAG, a recognized Smo agonist, and analyzed its effect on cell differentiation *in vitro*. In the differentiation assays, T3 (tri-iodothyronine) was added to the culture medium to enhance differentiation (Figure 6A). In the control group treated with DMSO, MBP was abundantly expressed 6 days after the initiation of differentiation (6 ddiff). However, SAG treatment notably hindered

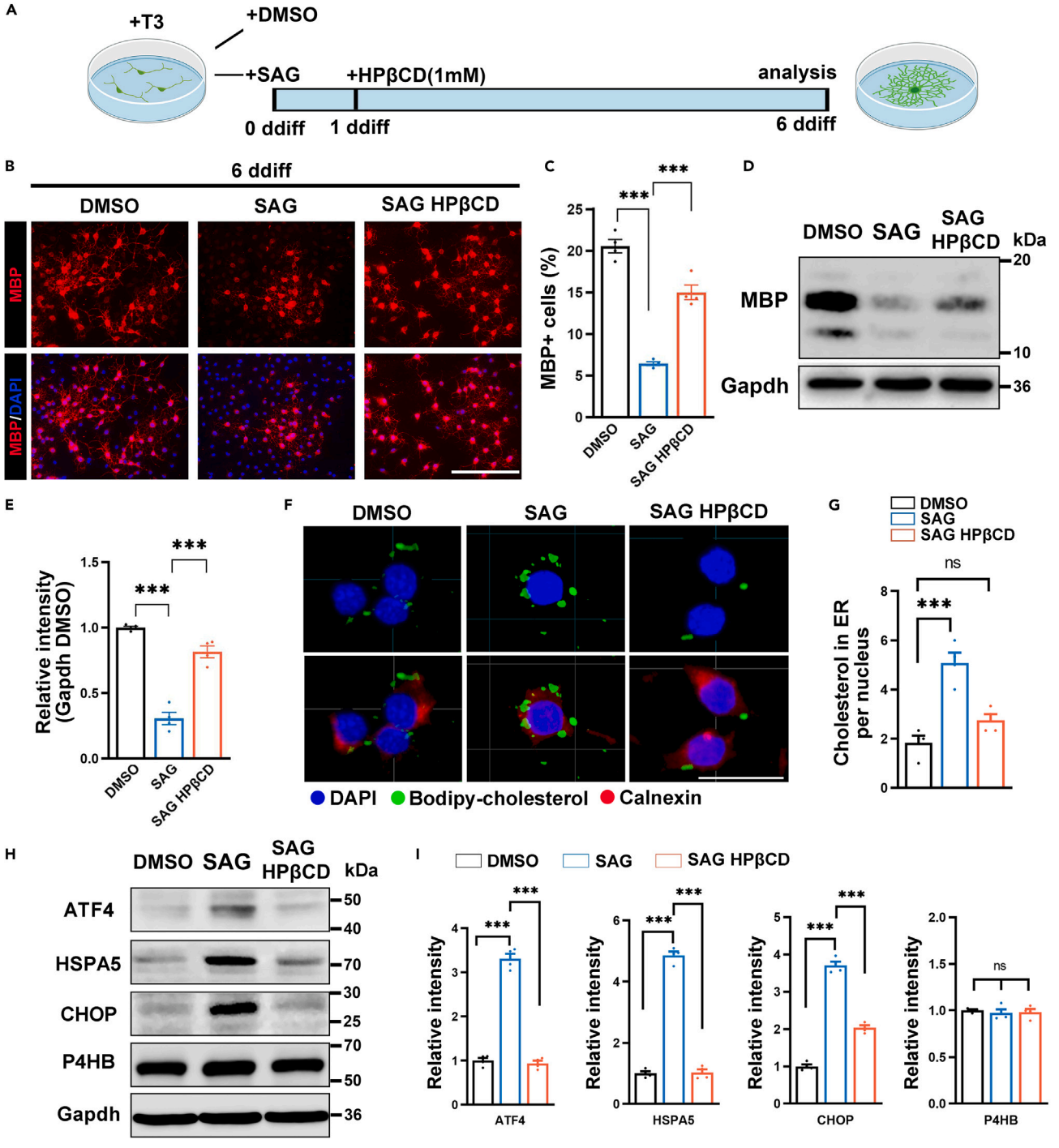

Figure 6. Smo agonist SAG inhibits OL differentiation *in vitro* via cholesterol accumulation in ER

(A) Experimental paradigm for SAG and HPβCD treatment in CG4 cells.

(B) Immunostaining of MBP in the differentiation medium with or without SAG or HPβCD treatment at 6 ddiff. Nuclei were stained with DAPI.

(C) Quantitative analysis of the proportion of MBP+ cells from (B).

(D) Western blot analyses of MBP expression from cells treated with or without SAG or HPβCD.

(E) Quantitative analyses of the relative expression levels of MBP from (D).

(F) Double immunostaining of BODIPY-cholesterol and Calnexin (red) in CG4 cells with or without SAG or HPβCD treatment. Scale bar: 10 μm.

Figure 6. *Continued*

(G) Quantification of cholesterol punctae in ER per nucleus from (F).

(H) Western blot analyses of the expression levels of ATF4, HSPA5, CHOP, P4HB from cells treated with or without SAG or HPβCD.

(I) Quantification of relative density from (H). Data are represented as mean ± *SEM*. For all statistical analysis, *p* values were calculated using one-way ANOVA with Dunnett's multiple-comparison correction. ***$p < 0.001$. ns: no significant difference. Scale bar: 10 μm.

cell differentiation, evident from the reduced proportion of MBP+ cells in this group (Figures 6B and 6C). Western blot analysis further confirmed the inhibition of MBP expression following SAG treatment (Figures 6D and 6E). Quantitative analyses revealed a significant upregulation of genes involved in cholesterol biosynthesis (*Mvk*, *Mvd*, *Fdft1*, *Scap* and *Srebf2*) in SAG-treated cells, while genes linked to cholesterol transportation (*Abcg4*, *Npc1*, *Npc2*, *Scp2*) remained unchanged (Figures S4A and S4B). Consistent with these findings, we observed a pronounced BODIPY-cholesterol signal within a 2-μm radius of the nuclei in SAG-treated cells (Figure 6F). In line with *in vivo* results, the addition of HPβCD to SAG-treated CG4 cells notably elevated the proportion of differentiated MBP+ OLs and mitigated cholesterol accumulation. Thus, our *in vitro* cell differentiation assays further corroborated that excessive activation of Hh signaling disrupted OL differentiation due to abnormal cholesterol accumulation.

Previous studies have indicated that lipid droplet accumulation is a hallmark of ER stress,[45,46] and ER stress can hinder cell differentiation.[47–51] Co-labeling of BODIPY-cholesterol with the ER marker Calnexin revealed that the majority of intracellular cholesterol in SAG-treated cells were stored in the ER (Figures 6F and 6G), suggesting a potential link between cholesterol dysregulation and ER stress. Furthermore, the expression of several ER stress-associated proteins (ATF4, HSPA5, CHOP) was significantly elevated in SAG-treated cells (Figures 6H and 6I). The addition of HPβCD to SAG-treated cells not only reduced the cholesterol accumulation in the ER, but also reduced the expression of ER stress-related proteins. Therefore, abnormal cholesterol accumulation is the primary cause of ER stress in SAG-treated cells. Based on these *in vivo* and *in vitro* findings, we conclude that hyperactivation of Hh signaling pathway boosts cholesterol biosynthesis in OPCs, leading to excess cholesterol accumulation, ER stress and ultimately, the inhibition of OL differentiation and myelination during development.

DISCUSSION

The study reveals an inhibitory role of Hh signaling in myelination and remyelination processes, specifically in brain OPCs. Activation of Hh signaling hinders OL differentiation and myelin formation during early developmental stages (Figures 1 and 2), without affecting OPC proliferation or migration. This observation stands in contrast to previous reports suggesting Hh activation fosters OPC proliferation. Some studies have shown that pharmacological activation of Smo with SAG can boost OPC proliferation and differentiation,[30,36] but this enhancement is not attributed to the direct activation of Hh signaling within the OL lineages. Instead, SAG exerts its influence on other cell types as well.[52] For instance, Laouarem et al. discovered that in the context of brain demyelination, SAG indirectly promotes OPC differentiation through microglia activity.[30] Echoing our findings, Nocera et al. also reported that Shh/Smo can impede OPC differentiation.[40] Although they inferred that constitutive activation of Shh/Smo pathway promotes the proliferation of OPCs during active demyelination, they only counted the total number of proliferating OPCs, without calculating the proliferation rate of OPCs. Thus, a direct conclusion cannot be drawn about promoting differentiation.

Furthermore, activation of Hh signaling in adult OPCs also reduced their differentiation capacity (Figure 3), which is unfavorable for myelin regeneration. The apparent inconsistency between our findings and earlier reports claiming that Smo agonist SAG promotes remyelination could be attributed to the different cell types targeted (resident OPCs versus NSCs). Previous research has predominantly focused on the role of Hh signaling in NSCs,[53,54] overlooking its effects on OPCs. While Smo-mediated signaling can induce the differentiation of SVZ-derived NSCs into OPCs and augment the proliferation of these NSC-derived OPCs,[53,54] prolonged exposure to Hh signaling may hinder OPC differentiation, as evidenced in our study In support of this, Nocera et al. demonstrate that during the Cuprizone-induced demyelination phase, Shh mainly stimulates early stage OPC proliferation, thereby expanding the pool of progenitor cells available for remyelination.[40] However, once OPCs reach a sufficient density, this pathway must be suppressed to allow for OPC differentiation.

In the context of MS and other neurodegenerative diseases, the phased activation of Hh signaling may play a crucial role. Wang et al. have demonstrated that Shh and its downstream transcription factor Gli1 are initially increased during early inflammation of active lesions of MS, meditating NSC differentiation. However, Gli1 was significantly decreased in spinal cord OPCs in chronic active and inactive lesions from MS brain. Therefore, understanding the phased effects of Hh signaling on OL development is essential for precise regulation and effective use of Hh agonists in MS treatment. Additionally, when considering Hh signaling activators in therapies, the potential cancer risk must be carefully managed,[55] as excessive Hh signaling is directly linked to a high incidence of tumors in Gorlin syndrome.[37] Thus, therapeutic strategies involving Hh signaling must delicately balance its beneficial effects with the risk of tumorigenesis, ensuring careful control over the duration and dosage of activation. Furthermore, the existence of non-canonical Smo signaling adds another layer of complexity. Recently, the Smo agonist GSA-10, which activates the non-canonical pathways associated with Gli1 inhibition, has been reported to promote remyelination.[56] Thus, non-canonical Hh signaling is able to promote remyelination until axon engagement. Fang et al., reviewed the remyelinating effects of various small molecules that bind to Smo, suggesting that different Smo agonists may activate distinct signaling pathways, potentially by binding to different sites on Smo.[34] Therefore, targeting specific components within the Hh signaling cascade could achieve beneficial outcomes while minimizing associated risks.

Currently, the mechanisms by which continuous activation of Hh signaling in OPCs impairs their terminal differentiation remains unclear. RNA-seq analyses of brain tissues have revealed a significant upregulation of genes related to cholesterol metabolism in SmoM2-OE mice

(Figures 4B–4D). Consistent with these findings, cholesterol staining in these mice showed a notable increase in the forebrain cortex and CC compared to control mice (Figures 4E–4G). Previous studies in other cell types have also documented a similar role of Hh signaling in cholesterol biosynthesis.[57,58] For instance, in osteoarthritis, Hh signaling has been identified as a modulator of genes that mediate cholesterol homeostasis in chondrocytes.[57] Additionally, Clobetasol, another Smo agonist,[59] up-regulates the expression of SREBFs in mouse ectodermal stem cell-derived OPCs (mEpiSC-OPCs),[58] further highlighting the involvement of Hh signaling in cholesterol biosynthesis.

Our findings further suggest that dysregulation of cholesterol in OLs impairs myelin formation (Figures 5D and 5G). Maintaining appropriate intracellular cholesterol levels is crucial for preserving the fluidity and integrity of myelin sheaths.[60–64] Dysregulation of cholesterol in these cells can lead to alteration in the myelin sheath and subsequent CNS dysfunction. Recent studies indicate that loss of mTOR, a key regulator of cholesterol synthesis in oligodendroglia, results in myelin deficits in adults, including impaired axonal function, spontaneous demyelination and OL death.[65] Consistent with our findings, Blanchard et al. discovered that APOE4 isoform, the most potent genetic predisposition for Alzheimer's disease, disrupts cholesterol and lipid transport.[66] This disruption leads to aberrant deposition of cholesterol in OLs, ultimately impairing myelin formation. Similarly, Yu et al. observed that mutation in the cholesterol transporter NPC1 results in Niemann-Pick type C, a childhood neurological disease marked by intracellular lipid deposition, axonal swelling and neuronal loss.[67] Knockdown of *Npc1* in OLs hinders cholesterol transport, blocks OL differentiation, and leads to defect myelination.[43,67,68] Notably, the cholesterol efflux agent cyclodextrin (HPβCD) used in these studies also remedied the myelin defects in SmoM2-OE mice.

Furthermore, we found that treatment of CG4 oligodendroglial cell line with SAG leads to cholesterol accumulation within the ER (Figure 6E), along with increased protein expression associated with the unfolded-protein-response (UPR) pathway.[69] Pharmacologically facilitating cholesterol transport could alleviate cholesterol deposition in the ER and downregulate UPR proteins. Previous studies indicate that OLs are highly sensitive to disturbance in ER homeostasis.[47–51] Pennuto et al. found that removal of the UPR-mediator CHOP improves motor functions and diminishes demyelination in Charcot-Marie-Tooth 1B mice.[48] Thus, it is quite possible that cholesterol accumulation and activation of ER-stress response might be responsible for defective OL differentiation and (re)myelination in SmoM2-OE mice.

Limitations of the study

Even though our study found that excessive activation of Hh signaling in OPCs upregulates cholesterol synthesis and leads to abnormal cholesterol accumulation in the ER, it is still unclear whether this directly results in increased cholesterol synthesis, the formation of intracellular lipid droplets, and the effects on cholesterol balance in other neural cells. Also, we acknowledge the limitations of this model; while LPC is useful for studying remyelination, it may not fully replicate the complexity of demyelinating diseases in humans.

RESOURCE AVAILABILITY

Lead contact

Further information and requests for resources and reagents should be directed to and will be fulfilled by the lead contact, X.X. (xiaofengxu@hznu.edu.cn).

Materials availability

This study did not generate new unique reagents.

Data and code availability

- The RNA-seq datasets have been deposited in Gene Expression Omnibus (GEO): GSE261881. They are publicly available as of the date of publication.
- This paper does not report original code.
- Any additional information required to reanalyzed the data reported in this paper is available for the lead contact upon request.

ACKNOWLEDGMENTS

This work was partially supported by grants from Brain Initiative Grant of the Ministry of Science and Technology, China (STI2030-Major Projects 2022ZD0204700), National Natural Science Foundation of China, China (82101244, 32170969), and Natural Science Foundation of Zhejiang Province, China (LY24C090006, LY22H090002).

AUTHOR CONTRIBUTIONS

X.X. conceived the study. M.Q. and X.X. supervised the study. M.Q., X.X., and M.F. designed the experiments. M.F., X.W., L.C., F.L., and S.W. performed experiments. L.S., H.Y., L.S., and X.W performed the quantitative analyses of the results. J.Y. provided unpublished reagents and analytical tools. M.Q., X.X., and M.F. analyzed data. M.F. wrote the first draft of the manuscript. M.Q. and X.X. revised the manuscript.

DECLARATION OF INTERESTS

The authors declare no competing interests.

STAR★METHODS

Detailed methods are provided in the online version of this paper and include the following:

- KEY RESOURCES TABLE
- EXPERIMENTAL MODEL AND STUDY PARTICIPANT DETAILS

SUPPLEMENTAL INFORMATION

Supplemental information can be found online at https://doi.org/10.1016/j.isci.2024.111016.

Received: June 19, 2024
Revised: August 9, 2024
Accepted: September 19, 2024
Published: September 23, 2024

REFERENCES

1. Nave, K.A. (2010). Myelination and support of axonal integrity by glia. Nature *468*, 244–252. https://doi.org/10.1038/nature09614.
2. Edgar, J.M., and Garbern, J. (2004). The myelinated axon is dependent on the myelinating cell for support and maintenance: molecules involved. J. Neurosci. Res. *76*, 593–598. https://doi.org/10.1002/jnr.20063.
3. Emery, B. (2010). Regulation of oligodendrocyte differentiation and myelination. Science *330*, 779–782. https://doi.org/10.1126/science.1190927.
4. Nave, K.A., Asadollahi, E., and Sasmita, A. (2023). Expanding the function of oligodendrocytes to brain energy metabolism. Curr. Opin. Neurobiol. *83*, 102782. https://doi.org/10.1016/j.conb.2023.102782.
5. Kole, K., Voesenek, B.J.B., Brinia, M.E., Petersen, N., and Kole, M.H.P. (2022). Parvalbumin basket cell myelination accumulates axonal mitochondria to internodes. Nat. Commun. *13*, 7598. https://doi.org/10.1038/s41467-022-35350-x.
6. Brécier, A., Li, V.W., Smith, C.S., Halievski, K., and Ghasemlou, N. (2023). Circadian rhythms and glial cells of the central nervous system. Biol. Rev. *98*, 520–539. https://doi.org/10.1111/brv.12917.
7. Jäkel, S., Agirre, E., Mendanha Falcão, A., van Bruggen, D., Lee, K.W., Knuesel, I., Malhotra, D., Ffrench-Constant, C., Williams, A., and Castelo-Branco, G. (2019). Altered human oligodendrocyte heterogeneity in multiple sclerosis. Nature *566*, 543–547. https://doi.org/10.1038/s41586-019-0903-2.
8. Yeung, M.S.Y., Djelloul, M., Steiner, E., Bernard, S., Salehpour, M., Possnert, G., Brundin, L., and Frisén, J. (2019). Dynamics of oligodendrocyte generation in multiple sclerosis. Nature *566*, 538–542. https://doi.org/10.1038/s41586-018-0842-3.
9. Elbaz, B., and Popko, B. (2019). Molecular control of oligodendrocyte development. Trends Neurosci. *42*, 263–277. https://doi.org/10.1016/j.tins.2019.01.002.
10. Tepavčević, V., and Lubetzki, C. (2022). Oligodendrocyte progenitor cell recruitment and remyelination in multiple sclerosis: the more, the merrier? Brain J. Neurol. *145*, 4178–4192. https://doi.org/10.1093/brain/awac307.
11. Gallo, V., and Deneen, B. (2014). Glial development: the crossroads of regeneration and repair in the CNS. Neuron *83*, 283–308. https://doi.org/10.1016/j.neuron.2014.06.010.
12. Pandey, S., Shen, K., Lee, S.H., Shen, Y.A.A., Wang, Y., Otero-García, M., Kotova, N., Vito, S.T., Laufer, B.I., Newton, D.F., et al. (2022). Disease-associated oligodendrocyte responses across neurodegenerative diseases. Cell Rep. *40*, 111189. https://doi.org/10.1016/j.celrep.2022.111189.
13. Zota, I., Chanoumidou, K., Charalampopoulos, I., and Gravanis, A. (2024). Dynamics of myelin deficits in the 5xFAD mouse model for Alzheimer's disease and the protective role of BDNF. Glia *72*, 809–827. https://doi.org/10.1002/glia.24505.
14. Festa, L.K., Grinspan, J.B., and Jordan-Sciutto, K.L. (2024). White matter injury across neurodegenerative disease. Trends Neurosci. *47*, 47–57. https://doi.org/10.1016/j.tins.2023.11.003.
15. Wang, F., Ren, S.Y., Chen, J.F., Liu, K., Li, R.X., Li, Z.F., Hu, B., Niu, J.Q., Xiao, L., Chan, J.R., and Mei, F. (2020). Myelin degeneration and diminished myelin renewal contribute to age-related deficits in memory. Nat. Neurosci. *23*, 481–486. https://doi.org/10.1038/s41593-020-0588-8.
16. Emery, B., and Lu, Q.R. (2015). Transcriptional and Epigenetic Regulation of Oligodendrocyte Development and Myelination in the Central Nervous System. Cold Spring Harbor Perspect. Biol. *7*, a020461. https://doi.org/10.1101/cshperspect.a020461.
17. Choudhry, Z., Rikani, A.A., Choudhry, A.M., Tariq, S., Zakaria, F., Asghar, M.W., Sarfraz, M.K., Haider, K., Shafiq, A.A., and Mobassarah, N.J. (2014). Sonic hedgehog signalling pathway: a complex network. Ann. Neurosci. *21*, 28–31. https://doi.org/10.5214/ans.0972.7531.210109.
18. Jessell, T.M. (2000). Neuronal specification in the spinal cord: inductive signals and transcriptional codes. Nat. Rev. Genet. *1*, 20–29. https://doi.org/10.1038/35049541.
19. Richardson, W.D., Pringle, N.P., Yu, W.P., and Hall, A.C. (1997). Origins of spinal cord oligodendrocytes: possible developmental and evolutionary relationships with motor neurons. Dev. Neurosci. *19*, 58–68. https://doi.org/10.1159/000111186.
20. Cai, J., Qi, Y., Hu, X., Tan, M., Liu, Z., Zhang, J., Li, Q., Sander, M., and Qiu, M. (2005). Generation of oligodendrocyte precursor cells from mouse dorsal spinal cord independent of Nkx6 regulation and Shh signaling. Neuron *45*, 41–53. https://doi.org/10.1016/j.neuron.2004.12.028.
21. Xiao, W.F., Li, Y.S., Deng, A., Yang, Y.T., and He, M. (2020). Functional role of hedgehog pathway in osteoarthritis. Cell Biochem. Funct. *38*, 122–129. https://doi.org/10.1002/cbf.3448.
22. Tan, M., Hu, X., Qi, Y., Park, J., Cai, J., and Qiu, M. (2006). Gli3 mutation rescues the generation, but not the differentiation, of oligodendrocytes in Shh mutants. Brain Res. *1067*, 158–163. https://doi.org/10.1016/j.brainres.2005.10.041.
23. Oh, S., Huang, X., and Chiang, C. (2005). Specific requirements of sonic hedgehog signaling during oligodendrocyte development. Dev. Dynam. *234*, 489–496. https://doi.org/10.1002/dvdy.20422.
24. Gibney, S.M., and McDermott, K.W. (2007). Differentiation of oligodendrocytes in neurospheres derived from embryonic rat brain using growth and differentiation factors. J. Neurosci. Res. *85*, 1912–1920. https://doi.org/10.1002/jnr.21331.
25. Gibney, S.M., and McDermott, K.W. (2009). Sonic hedgehog promotes the generation of myelin proteins by transplanted oligosphere-derived cells. J. Neurosci. Res. *87*, 3067–3075. https://doi.org/10.1002/jnr.22138.

26. Loulier, K., Ruat, M., and Traiffort, E. (2006). Increase of proliferating oligodendroglial progenitors in the adult mouse brain upon Sonic hedgehog delivery in the lateral ventricle. J. Neurochem. *98*, 530–542. https://doi.org/10.1111/j.1471-4159.2006.03896.x.
27. Merchán, P., Bribián, A., Sánchez-Camacho, C., Lezameta, M., Bovolenta, P., and de Castro, F. (2007). Sonic hedgehog promotes the migration and proliferation of optic nerve oligodendrocyte precursors. Mol. Cell. Neurosci. *36*, 355–368. https://doi.org/10.1016/j.mcn.2007.07.012.
28. Ortega, M.C., Cases, O., Merchán, P., Kozyraki, R., Clemente, D., and de Castro, F. (2012). Megalin mediates the influence of sonic hedgehog on oligodendrocyte precursor cell migration and proliferation during development. Glia *60*, 851–866. https://doi.org/10.1002/glia.22316.
29. Rowitch, D.H., S-Jacques, B., Lee, S.M., Flax, J.D., Snyder, E.Y., and McMahon, A.P. (1999). Sonic hedgehog regulates proliferation and inhibits differentiation of CNS precursor cells. J. Neurosci. *19*, 8954–8965.
30. Laouarem, Y., Kassoussi, A., Zahaf, A., Hutteau-Hamel, T., Mellouk, A., Bobé, P., Mattern, C., Schumacher, M., and Traiffort, E. (2021). Functional cooperation of the hedgehog and androgen signaling pathways during developmental and repairing myelination. Glia *69*, 1369–1392. https://doi.org/10.1002/glia.23967.
31. Wang, L.C., and Almazan, G. (2016). Role of Sonic hedgehog signaling in oligodendrocyte differentiation. Neurochem. Res. *41*, 3289–3299. https://doi.org/10.1007/s11064-016-2061-3.
32. Xu, X., Yu, Q., Fang, M., Yi, M., Yang, A., Xie, B., Yang, J., Zhang, Z., Dai, Z., and Qiu, M. (2020). Stage-specific regulation of oligodendrocyte development by Hedgehog signaling in the spinal cord. Glia *68*, 422–434. https://doi.org/10.1002/glia.23729.
33. Wang, Y., Imitola, J., Rasmussen, S., O'Connor, K.C., and Khoury, S.J. (2008). Paradoxical dysregulation of the neural stem cell pathway sonic hedgehog-Gli1 in autoimmune encephalomyelitis and multiple sclerosis. Ann. Neurol. *64*, 417–427. https://doi.org/10.1002/ana.21457.
34. Fang, M., Tang, T., Qiu, M., and Xu, X. (2022). Hedgehog signaling in CNS remyelination. Cells *11*, 2260. https://doi.org/10.3390/cells11142260.
35. Gao, H., Guo, Y., Biswas, S., Li, J., Zhang, H., Chen, Z., and Deng, W. (2022). Promoting oligodendrocyte differentiation from Human induced pluripotent stem cells by activating Endocannabinoid signaling for treating spinal cord injury. Stem Cell Rev. Rep. *18*, 3033–3049. https://doi.org/10.1007/s12015-022-10405-0.
36. Sanchez, M.A., Sullivan, G.M., and Armstrong, R.C. (2018). Genetic detection of Sonic hedgehog (Shh) expression and cellular response in the progression of acute through chronic demyelination and remyelination. Neurobiol. Dis. *115*, 145–156. https://doi.org/10.1016/j.nbd.2018.04.003.
37. Kantarci, M., Ertas, U., Alper, F., Sutbeyaz, Y., Karasen, R.M., and Onbas, O. (2003). Gorlin's syndrome with a thin corpus callosum and a third ventricular cyst. Neuroradiology *45*, 390–392. https://doi.org/10.1007/s00234-003-0988-y.
38. Namchaiw, P., Wen, H., Mayrhofer, F., Chechneva, O., Biswas, S., and Deng, W. (2019). Temporal and partial inhibition of GLI1 in neural stem cells (NSCs) results in the early maturation of NSC derived oligodendrocytes in vitro. Stem Cell Res. Ther. *10*, 272. https://doi.org/10.1186/s13287-019-1374-y.
39. Radecki, D.Z., Messling, H.M., Haggerty-Skeans, J.R., Bhamidipati, S.K., Clawson, E.D., Overman, C.A., Thatcher, M.M., Salzer, J.L., and Samanta, J. (2020). Relative levels of *Gli1* and *Gli2* determine the response of ventral neural stem cells to demyelination. Stem Cell Rep. *15*, 1047–1055. https://doi.org/10.1016/j.stemcr.2020.10.003.
40. Nocera, S., Marchena, M.A., Fernández-Gómez, B., Gómez-Martín, P., Sánchez-Jiménez, E., Macías-Castellano, A., Laó, Y., Cordano, C., Gómez-Torres, Ó., Luján, R., and de Castro, F. (2024). Activation of Shh/Smo is sufficient to maintain oligodendrocyte precursor cells in an undifferentiated state and is not necessary for myelin formation and (re)myelination. Glia *72*, 1469–1483. https://doi.org/10.1002/glia.24540.
41. Xie, J., Murone, M., Luoh, S.M., Ryan, A., Gu, Q., Zhang, C., Bonifas, J.M., Lam, C.W., Hynes, M., Goddard, A., et al. (1998). Activating smoothened mutations in sporadic basal-cell carcinoma. Nature *391*, 90–92. https://doi.org/10.1038/34201.
42. Abi-Mosleh, L., Infante, R.E., Radhakrishnan, A., Goldstein, J.L., and Brown, M.S. (2009). Cyclodextrin overcomes deficient lysosome-to-endoplasmic reticulum transport of cholesterol in niemann-pick type C cells. Proc. Natl. Acad. Sci. USA *106*, 19316–19321. https://doi.org/10.1073/pnas.0910916106.
43. Kunkel, T.J., Townsend, A., Sullivan, K.A., Merlet, J., Schuchman, E.H., Jacobson, D.A., and Lieberman, A.P. (2023). The cholesterol transporter NPC1 is essential for epigenetic regulation and maturation of oligodendrocyte lineage cells. Nat. Commun. *14*, 3964. https://doi.org/10.1038/s41467-023-39733-6.
44. Singhal, A., Krystofiak, E.S., Jerome, W.G., and Song, B. (2020). 2-hydroxypropyl-gamma-cyclodextrin overcomes NPC1 deficiency by enhancing lysosome-ER association and autophagy. Sci. Rep. *10*, 8663. https://doi.org/10.1038/s41598-020-65627-4.
45. Kamińska, D., and Skrzycki, M. (2024). Lipid droplets, autophagy, and ER stress as key (survival) pathways during ischemia-reperfusion of transplanted grafts. Cell Biol. Int. *48*, 253–279. https://doi.org/10.1002/cbin.12114.
46. Ye, J., Rawson, R.B., Komuro, R., Chen, X., Davé, U.P., Prywes, R., Brown, M.S., and Goldstein, J.L. (2000). ER stress induces cleavage of membrane-bound ATF6 by the same proteases that process SREBPs. Mol. Cell *6*, 1355–1364. https://doi.org/10.1016/S1097-2765(00)00133-7.
47. Bauer, J., Bradl, M., Klein, M., Leisser, M., Deckwerth, T.L., Wekerle, H., and Lassmann, H. (2002). Endoplasmic reticulum stress in PLP-overexpressing transgenic rats: gray matter oligodendrocytes are more vulnerable than white matter oligodendrocytes. J. Neuropathol. Exp. Neurol. *61*, 12–22. https://doi.org/10.1093/jnen/61.1.12.
48. Pennuto, M., Tinelli, E., Malaguti, M., Del Carro, U., D'Antonio, M., Ron, D., Quattrini, A., Feltri, M.L., and Wrabetz, L. (2008). Ablation of the UPR-mediator CHOP restores motor function and reduces demyelination in Charcot-Marie-Tooth 1B mice. Neuron *57*, 393–405. https://doi.org/10.1016/j.neuron.2007.12.021.
49. Wrabetz, L., D'Antonio, M., Pennuto, M., Dati, G., Tinelli, E., Fratta, P., Previtali, S., Imperiale, D., Zielasek, J., Toyka, K., et al. (2006). Different intracellular pathomechanisms produce diverse myelin protein zero neuropathies in transgenic mice. J. Neurosci. *26*, 2358–2368. https://doi.org/10.1523/JNEUROSCI.3819-05.2006.
50. Van der Voorn, J.P., van Kollenburg, B., Bertrand, G., Van Haren, K., Scheper, G.C., Powers, J.M., and van der Knaap, M.S. (2005). The unfolded protein response in vanishing white matter disease. J. Neuropathol. Exp. Neurol. *64*, 770–775. https://doi.org/10.1097/01.jnen.0000178446.41595.3a.
51. Southwood, C.M., Garbern, J., Jiang, W., and Gow, A. (2002). The unfolded protein response modulates disease severity in Pelizaeus-Merzbacher disease. Neuron *36*, 585–596. https://doi.org/10.1016/s0896-6273(02)01045-0.
52. Miron, V.E., Boyd, A., Zhao, J.W., Yuen, T.J., Ruckh, J.M., Shadrach, J.L., van Wijngaarden, P., Wagers, A.J., Williams, A., Franklin, R.J.M., and Ffrench-Constant, C. (2013). M2 microglia and macrophages drive oligodendrocyte differentiation during CNS remyelination. Nat. Neurosci. *16*, 1211–1218. https://doi.org/10.1038/nn.3469.
53. Balordi, F., and Fishell, G. (2007). Hedgehog signaling in the subventricular zone is required for both the maintenance of stem cells and the migration of newborn neurons. J. Neurosci. *27*, 5936–5947. https://doi.org/10.1523/JNEUROSCI.1040-07.2007.
54. Tong, C.K., Fuentealba, L.C., Shah, J.K., Lindquist, R.A., Ihrie, R.A., Guinto, C.D., Rodas-Rodriguez, J.L., and Alvarez-Buylla, A. (2015). A dorsal SHH-dependent domain in the V-SVZ produces large numbers of oligodendroglial lineage cells in the postnatal brain. Stem Cell Rep. *5*, 461–470. https://doi.org/10.1016/j.stemcr.2015.08.013.
55. Krenn, P.W., and Aberger, F. (2023). Targeting cancer hallmark vulnerabilities in hematologic malignancies by interfering with Hedgehog/GLI signaling. Blood *142*, 1945–1959. https://doi.org/10.1182/blood.2021014761.
56. Del Giovane, A., Russo, M., Tirou, L., Faure, H., Ruat, M., Balestri, S., Sposato, C., Basoli, F., Rainer, A., Kassoussi, A., et al. (2021). Smoothened/AMP-Activated Protein Kinase Signaling in Oligodendroglial Cell Maturation. Front. Cell. Neurosci. *15*, 801704. https://doi.org/10.3389/fncel.2021.801704.
57. Ali, S.A., Al-Jazrawe, M., Ma, H., Whetstone, H., Poon, R., Farr, S., Naples, M., Adeli, K., and Alman, B.A. (2016). Regulation of cholesterol homeostasis by hedgehog signaling in Osteoarthritic Cartilage. Arthritis Rheumatol. *68*, 127–137. https://doi.org/10.1002/art.39337.
58. Ashikawa, Y., Nishimura, Y., Okabe, S., Sasagawa, S., Murakami, S., Yuge, M., Kawaguchi, K., Kawase, R., and Tanaka, T. (2016). Activation of sterol regulatory element binding factors by fenofibrate and gemfibrozil Stimulates myelination in zebrafish. Front. Pharmacol. *7*, 206. https://doi.org/10.3389/fphar.2016.00206.
59. Yao, X., Su, T., and Verkman, A.S. (2016). Clobetasol promotes remyelination in a mouse model of neuromyelitis optica. Acta Neuropathol. Commun. *4*, 42. https://doi.org/10.1186/s40478-016-0309-4.

60. Saher, G., and Stumpf, S.K. (2015). Cholesterol in myelin biogenesis and hypomyelinating disorders. Biochim. Biophys. Acta *1851*, 1083–1094. https://doi.org/10.1016/j.bbalip.2015.02.010.

61. Cantuti-Castelvetri, L., Fitzner, D., Bosch-Queralt, M., Weil, M.T., Su, M., Sen, P., Ruhwedel, T., Mitkovski, M., Trendelenburg, G., Lütjohann, D., et al. (2018). Defective cholesterol clearance limits remyelination in the aged central nervous system. Science *359*, 684–688. https://doi.org/10.1126/science.aan4183.

62. Saher, G., Brügger, B., Lappe-Siefke, C., Möbius, W., Tozawa, R.i., Wehr, M.C., Wieland, F., Ishibashi, S., and Nave, K.A. (2005). High cholesterol level is essential for myelin membrane growth. Nat. Neurosci. *8*, 468–475. https://doi.org/10.1038/nn1426.

63. Morell, P., and Jurevics, H. (1996). Origin of cholesterol in myelin. Neurochem. Res. *21*, 463–470. https://doi.org/10.1007/BF02527711.

64. O'brien, J.S. (1965). Stability of the myelin membrane. Science *147*, 1099–1107. https://doi.org/10.1126/science.147.3662.1099.

65. Khandker, L., Jeffries, M.A., Chang, Y.J., Mather, M.L., Evangelou, A.V., Bourne, J.N., Tafreshi, A.K., Ornelas, I.M., Bozdagi-Gunal, O., Macklin, W.B., and Wood, T.L. (2022). Cholesterol biosynthesis defines oligodendrocyte precursor heterogeneity between brain and spinal cord. Cell Rep. *38*, 110423. https://doi.org/10.1016/j.celrep.2022.110423.

66. Blanchard, J.W., Akay, L.A., Davila-Velderrain, J., Von Maydell, D., Mathys, H., Davidson, S.M., Effenberger, A., Chen, C.Y., Maner-Smith, K., Hajjar, I., et al. (2022). APOE4 impairs myelination via cholesterol dysregulation in oligodendrocytes. Nature *611*, 769–779. https://doi.org/10.1038/s41586-022-05439-w.

67. Yu, T., and Lieberman, A.P. (2013). Npc1 acting in neurons and glia is essential for the formation and maintenance of CNS myelin. PLoS Genet. *9*, e1003462. https://doi.org/10.1371/journal.pgen.1003462.

68. Madra, M., and Sturley, S.L. (2010). Niemann-Pick type C pathogenesis and treatment: from statins to sugars. Clin. Lipidol. *5*, 387–395. https://doi.org/10.2217/clp.10.19.

69. Ron, D., and Walter, P. (2007). Signal integration in the endoplasmic reticulum unfolded protein response. Nat. Rev. Mol. Cell Biol. *8*, 519–529. https://doi.org/10.1038/nrm2199.

70. Fang, M., Yu, Q., Ou, B., Huang, H., Yi, M., Xie, B., Yang, A., Qiu, M., and Xu, X. (2020). Genetic evidence that dorsal spinal oligodendrocyte progenitor cells are capable of myelinating ventral axons effectively in mice. Neurosci. Bull. *36*, 1474–1483. https://doi.org/10.1007/s12264-020-00593-5.

STAR★METHODS

KEY RESOURCES TABLE

REAGENT or RESOURCE	SOURCE	IDENTIFIER
Antibodies		
anti-tdTomato/mCherry	Oasis Biofarm	Cat#OB-PRT017; RRID:AB_2934238
anti-ASPA	Oasis Biofarm	Cat#OB-PRT005; RRID:AB_2938679
anti-Calnexin	Santa Cruz	Cat#SC-11397; RRID:AB_2243890
anti-CC1	Oasis Biofarm	Cat#OB-PGP027; RRID:AB_2938820
anti-GFAP	Oasis Biofarm	Cat#OB-PRT001; RRID:AB_2938934
anti-IBA1	Oasis Biofarm	Cat#OB-MMS039; RRID:AB_2940798
anti-Ki67	Abcam	Cat#ab15580; RRID:AB_805388
anti-MBP	Oasis Biofarm	Cat#OB-PRB130; RRID:AB_2941876
anti-NG2	Oasis Biofarm	Cat#OB-PGP002; RRID:AB_2938678
anti-SOX10	Oasis Biofarm	Cat#OB-PRB053; RRID:AB_2934229
Goat-anti-MouseIgG1-594	Invitrogen	Cat#A21125; RRID:AB_2535767
Goat-anti-MouseIgG1-488	Invitrogen	Cat#A21121; RRID:AB_2535764
Goat-anti-MouseIgG H + L -633	Invitrogen	Cat#A21050; RRID:AB_2535718
Goat-anti-Rabbit-594	Invitrogen	Cat#A11012; RRID:AB_2758362
Goat-anti-Rabbit-488	Invitrogen	Cat#A11034; RRID:AB_2576217
Goat-anti-Rabbit-633	Invitrogen	Cat#A21070; RRID:AB_2535731
Goat-anti-GuineaPig-594	Invitrogen	Cat#A11076; RRID:AB_2534120
Goat-anti-GuineaPig-488	Invitrogen	Cat#A11073; RRID:AB_2534117
Goat-anti-GuineaPig-647	Oasis Biofarm	Cat#GP647; RRID:AB_3106973
Goat-anti-Rat-594	Invitrogen	Cat#A11007; RRID:AB_10561522
Goat-anti-Rat-488	Invitrogen	Cat#A11006; RRID:AB_2534074
Goat-anti-Rat-647	Oasis Biofarm	Cat#RT647;
Chemicals, peptides, and recombinant proteins		
Tamoxifen	Sigma-Aldrich	Cat#T5648
BrdU	Sigma-Aldrich	Cat#B5002
SAG	Sigma-Aldrich	Cat#566661
LPC	Sigma-Aldrich	Cat# L1381
HPβCD	MCE	Cat#128446-35-5
Penicillin-Streptomycin	Gibco	Cat#15140148
DMEM/F12	Gibco	Cat#C11330500BT
N2	Gibco	Cat#A1370701
B27	Gibco	Cat#A17504044
PDGF-AA	PeproTech	Cat#100-13A
BODIPY-Cholesterol (488)	Sigma-Aldrich	Cat#878557-19-8
triiodothyronine (T3)	Sigma-Aldrich	Cat# T6397
Critical commercial assays		
Enhanced chemiluminescence (ECL) detection system	Thermo Scientific	Cat#32109
TrueGold myelin staining Kit	Oasis Biofarm	Cat#BK-AC001
Deposited data		
Mouse: mRNA-seq data	This paper	GEO: GSE261881

(*Continued on next page*)

Continued

REAGENT or RESOURCE	SOURCE	IDENTIFIER
Experimental models: Cell lines		
Rat: CG4 line	ATCC	RRID: CVCL_0210
Experimental models: Organisms/strains		
Mouse: Gt(ROSA)26Sortm1(Smo/EYFP)Amc/J	The Jackson Laboratory	Cat#005130; RRID: IMSR_JAX:005130
Mouse: B6.Cg-Gt(ROSA)26Sortm9(CAG-tdTomato)Hze/J	The Jackson Laboratory	Cat#007909; RRID:IMSR_JAX:007909
Mouse: B6N.Cg-Tg(Pdgfra-cre/ERT)467Dbe/J	The Jackson Laboratory	Cat#018280; RRID: IMSR_JAX:018280
Oligonucleotides		
Oligonucleotides for genotyping	See Table S1	N/A
Oligonucleotides for RT-qPCR analysis	See Table S2	N/A
Software and algorithms		
GraphPad Prism 9.0	Graphpad	RRID: SCR_002798
ZESIS ZEN	Zesis	RRID: SCR_013672
Adobe Photoshop CS6	Adobe	RRID: SCR_014199
ImageJ	N/A	RRID: SCR_003070

EXPERIMENTAL MODEL AND STUDY PARTICIPANT DETAILS

Animal

All research protocols using animals were approved by the Institutional Animal Care and Use Committee at Hangzhou Normal University. Mice were bred in specific pathogen-free facilities at Hangzhou Normal University, and kept under standard housing conditions including a 12-h light/12-h dark cycle, with unlimited access to water and food. To ensure inclusivity, both sexes were equally used in all experiments. The mice utilized in this study were previously characterized.[32] *Rosa-SmoM2* (Stock No. 005130), *Rosa-tdTomato* (Stock No. 007909) and *PDGFRa-creERT2* (Stock No. 018280) were obtained from the Jackson Laboratory and maintained under C57BL/6 background. *PDGFRα-creERT2* line were mated with *Rosa-SmoM2* and *Rosa-tdTomato* to generate double or triple transgenic mice. Genotyping was performed by PCR using genomic DNA extracted from ear or toe biopsies. Primers used for genotyping are listed in Table S1. In this study, P15 mice were employed for investigations on OL development, while 8-week adult mice were utilized for the study of remyelination.

METHOD DETAILS

Cell culture

Rat CG4 cells were plated into a poly-L-lysine-coated glass coverslips at a density of 10,000 cells per cm^2 with DMEM/F12 (Gibco, Cat#C11330500BT) supplemented with N2 (Gibco, Cat#A1370701), B27 (Gibco, Cat#A17504044) and 10 ng/mL PDGF-AA (PeproTech, Cat#100-13A). To induce differentiation, the medium was substituted with DMEM/F12 medium with N2, B27 and 40 ng/mL triiodothyronine (T3) (Sigma-Aldrich, Cat# T6397). All cells were kept up in a humidified incubator with 5% CO_2 at 37°C, and replacement of the medium every two days.

Lysolecithin (LPC) lesion

Focal demyelinating lesions were performed in the CC of 8-week-old SmoM2-OE and control mice. 2 μL of 1% LPC (Sigma-Aldrich, Cat# L1381) was slowly injected into the corpus callosum (AP: 0.80 mm; ML: 0.1 mm; DV: 0.22 mm relative to bregma). Mice were allowed to recover and sacrificed at 7, 14 and 21 days post lesion (dpl).

Tamoxifen injection

Tamoxifen (Sigma-Aldrich, Cat#T5648) was dissolved in a solution of 90% corn oil and 10% ethanol at a concentration of 20 mg/mL. To induce SmoM2 overexpression in OPCs, Tamoxifen was administrated to SmoM2-OE and control mice through intraperitoneal injection at a dosage of 100 mg/kg (body weight). To investigate the effect of Hh signaling hyperactivation during development, Tamoxifen was injected to nursing female mice starting from P5. For the remyelination assays, both SmoM2-OE and control mice received tamoxifen injection for five days prior to LPC injury, and two days after LPC injury.

Immunofluorescence staining

SmoM2-OE and control mice at defined stages were deeply anesthetized and perfused with ice-cold PBS and then 4% polyformaldehyde (PFA). The brains were dissected and post-fixed in PFA overnight at 4°C, and then transferred into 30% sucrose in 1×PBS overnight. After dehydration, the tissues were then embedded in OCT Compound (Sakura Finetek) and sectioned on a cryostat with 14–16 μm thickness. Immunofluorescence staining was conducted as described previously,[70] with slight modifications. Cryosections were blocked in blocking buffer containing 5% goat serum and 0.1% Triton X- for 1 house at room temperature (RT), and then incubated with primary antibodies overnight at 4°C. Following 3 washes in PBS, sections were incubated with Alexa Fluor 488 or Alexa Fluor 594 secondary antibodies for 1 h at RT. Nuclear labeling was achieved by staining the slices with DAPI for 5 min. Images were taken by a Leica DMI600B inverted microscope. All experiments were independently repeated at least three times.

RNA *in situ* hybridization

RNA *in situ* hybridization was conducted as reported previously.[32] Cryosections was hybridized with digoxigenin (DIG)-labeled probes in a humidified, sealed container at 60°C overnight. The DIG-labeled RNA probe was synthesized through *in vitro* transcription kit utilizing T3/T7 RNA polymerase (Promega, Cat# P2803/P2077), diluted in hybridization buffer, and denatured at 85°C before use. After overnight hybridization, the sections were blocked in blocking buffer containing 10% sheep serum for 1 h at RT, and incubated with anti-DIG-AP antibody (Roche, Cat# 11093274910) at 4°C overnight. The color reaction was performed using NBI-BCIP kit (Roche, Cat#11681451001). Images were taken by a Nikon Eclipse 90i microscopy.

5-Bromo-2′-deoxyuridine (BrdU) treatment

BrdU (Sigma-Aldrich, Cat#B5002) was prepared at a concentration of 10 mg/mL in sterile 1× PBS and administered to mice via intraperitoneal injection at a dose of 100 μg/g body weight, 2 h prior to sample collection. For immunofluorescence labeling with the BrdU antibody, the samples were treated with 2 M HCl, incubated for 30 min at room temperature, and then processed according to standard immunofluorescence protocols.

TrueGold myelin staining

For TrueGold myelin staining, the cryosections were baked for 30 min at 37°C and then incubated with TrueGold myelin staining solution (Oasis Biofarm, Cat#BK-AC001) for 20–30 min at 45°C. After staining, the slides were rinsed with deionized water and incubated with thiosulfate solution for 2–3 min at 45°C. Images were taken by a Nikon Eclipse 90i microscopy.

Transmission electron microscopy (TEM)

TEM was performed as reported previously.[70] The corpus callosum samples were fixed first by 2.5% glutaraldehyde for 4 h and then by 1% osmium tetroxide (in 0.1M pH 7.0 phosphate buffer) for 2 h at RT. Then samples were then dehydrated by graded ethanol series (50%, 70%, 80%, 90%, 95% and 100%) and pure acetone for 20 min at RT. An embedding of these samples into Epon 812 resin and a heating polymerization under 60°C were done to obtain solid blocks. Ultra-thin sections (70 nm) of thee sample blocks were cut by a Leica UC 6 microtome with diamond knife. After double stained by uranyl acetate and lead citrate for 15 min, sections were put into an H-7650 TEM for observation. Total axons were counted per area in the CC of SmoM2-OE and control mice at P15.

RNA-seq and data analysis

RNA extraction, cDNA synthesiss, library construction and sequencing were performed at Shanghai Majorbio Bio-pharm Biotechnology Co., Ltd (Shanghai, China).The transcriptomic libraries were prepared using the TruSeq RNA Sample Preparation Kit (Illumina, USA) with 1 μg of total RNA. Sequencing was carried out on the Illumina NovaSeq 6000 sequencer. The RNA-seq datasets have been archived in GEO and can be assessed via the accession number GSE261881. To identify differentially expressed genes (DEGs) upon SmoM2 overexpression, the expression level of each gene was calculated according to the transcripts per million reads (TPM) method. Differential expression analyses were conducted using DESeq2. DEGs with log2-fold ≥ 1 and p-adjust < 0.05 were considered to be significantly differentially expressed genes. Gene ontology (GO) analysis was performed to identify which DEGs were significantly enriched in GO terms compared with whole-transcriptome background and carried out by Goatools (http://github.com/tanghaibao/Goatools).

HPβCD treatment

HPβCD (MCE, CAS#128446-35-5) was intraperitoneally injected into SmoM2-OE and control mice at a dosage of 4,000 mg/kg. Some mice received saline injections as a vehicle control. For cell culture, HPβCD was added to the culture medium at a final concentration of 1 mM.

BODIPY-cholesterol staining

Tissue slides and cell coverslides were incubated with PBS containing 1 μg/mL BODIPY-cholesterol dye (Sigma-Aldrich, Cat#878557-19-8) for 20 min. After staining, slides were rinsed three times with PBS. Images were taken by Zeiss LSM710 confocal microscopy under 63× high

magnification, using the same parameters for different slides. While co-labeled with other marker genes, BODIPY-cholesterol dye was mixed directly with primary antibodies.

Western blot

Brain tissues from deeply anesthetized mice were dissected and homogenized. The tissues were lysed overnight at 4°C in lysis buffer (25 mM Tris-HCl, pH 7.4, 150 mM NaCl, 1% NP40, 0.5% Triton X-100, 1 mM EDTA) supplemented with protease inhibitor cocktail (Sigma-Aldrich, Cat#P0044). For cell cultures, each well of 6-well plates was rinsed in PBS and lysed in chilled lysis buffer on ice for 30 min. The lysates then underwent centrifugation at 12,000×g for 15 min at 4°C. Concentration of the supernatants was measured by BCA assay. A total of 20 μg protein was leaded onto an SDS-PAGE gel and subsequently transferred to PVDF membrane (Millipore, ISEQ00010). The membranes were blocked with a 5% nonfat milk solution in TBST for 1 h at RT and subsequently incubated with primary antibodies overnight at 4°C. After rinsing four times with TBST, the membranes were then incubated with HPR-conjugated secondary antibody for 1 h at RT. Proteins were detected using an ECL detection system (Thermo-Scientific, Cat#32109) and X-ray film.

Real-time quantitative PCR (qRT-PCR)

Total RNA was harvested from CG4 cells using TRIZOL Reagent (Invitrogen, Cat#15596026) according to the manufacturer's instruction and genomic DNA was removed using DNase I (Takara, Cat#2270A). The first-strand cDNA was synthesized from 1μg of total RNA using HiScript III 1st Strand cDNA Synthesis Kit (Vazyme, Cat#R312). The quantitative PCR experiments were performed using ChamQ Universal SYBR MasterMix (Vazyme, Cat#Q711-02) according to the manufacturer's instruction. Relative expression levels were calculated using the $2^{-\Delta\Delta Ct}$ approach. Primers used for qRT-PCR are listed in Table S2.

QUANTIFICATION AND STATISTICAL ANALYSIS

Results from independent animals, experiments or separately generated samples were treated as biological replicates, and allocating animals/samples to treatment by randomization procedure. The number of samples per group was $n \geq 3$ for all mice. All data were analyzed using Prism GraphPad 9.0 and presented as mean ± *SEM*. Unpaired two-tailed Student's t test was used for analysis between two groups with one variable. For comparisons involving more than two samples, significance was determined via one-way ANOVA with Dunnett's multiple-comparison correction. Statistical significance was set at $^{*}p < 0.05$; $^{**}p < 0.01$, $^{***}p < 0.001$.